Perovskite Nanoparticles

A General Soft-Chemistry Route to Perovskites and Related Materials: Synthesis of $BaTiO_3$, $BaZrO_3$, and $LiNbO_3$ Nanoparticles**

Markus Niederberger, Nicola Pinna, Julien Polleux, and Markus Antonietti*

Perovskites and related compounds are one of the most widely investigated classes of materials in solid-state chemistry because of their ferroelectric properties, which find a wide variety of applications in nonlinear optics, thin-film capaci-

[*] Dr. M. Niederberger, J. Polleux, Prof. Dr. M. Antonietti
Max Planck Institute of Colloids and Interfaces
Department of Colloid Chemistry
MPI Research Campus Golm
14424 Potsdam (Germany)
Fax: (+49) 331-567-9502
E-mail: markus.niederberger@mpikg-golm.mpg.de
Dr. N. Pinna
Fritz-Haber-Institute of the MPG
Department of Inorganic Chemistry
Faradayweg 4–6, 14195 Berlin (Germany)

[**] Financial support by the Max-Planck-Society is gratefully acknowledged.

  DOI: 10.1002/ange.200353300

tors, pyroelectric detectors, optical memories, and electro-optic modulators.[1] Most perovskite phases are still prepared by conventional solid-state reactions between the corresponding oxides or oxides and carbonates at temperatures above 1000 °C. However, wet-chemical methods are a promising alternative, because they can be better controlled from the molecular precursor to the final material to give highly pure and homogeneous materials, and allow low reaction temperatures to be used, the size and morphology of the particles to be controlled, and metastable phases be prepared. Sol–gel methods based on the hydrolysis of metal alkoxides have attracted much attention.[2,3] However, the development of soft-chemistry routes for the synthesis of perovskite nanocrystals only started a few years ago. Most preparations of $BaTiO_3$ use a titanium alkoxide or oxide as titanium source and barium salts such as barium halides, acetates, nitrates, or hydroxides.[4–7] The use of the stabilizing agent oleic acid allows the synthesis of crystalline $BaTiO_3$ nanoparticles with diameters ranging from 6 to 12 nm.[8] In comparison to $BaTiO_3$, the preparation of nanosized $LiNbO_3$ and $BaZrO_3$ has been much less investigated. Nanocrystalline $LiNbO_3$ with grain sizes of less than 10 nm was obtained by a wet-chemical method with a polymer-precursor technique and a double-alkoxide sol–gel method.[9] $BaZrO_3$ nanoparticles with diameters in the range of 30–40 nm were synthesized by sol–gel processes.[3] A urea-induced precipitation process led to $BaZrO_3$ nanoparticles with diameters around 90 nm.[10]

Herein we present a novel nonaqueous and low-temperature route to nanocrystalline ABO_3 compounds. To prove the generality of the synthetic approach, we prepared $BaTiO_3$ and $BaZrO_3$ as representatives of the perovskite family, and $LiNbO_3$ with the ilmenite structure. All of these materials have been intensively studied because of their outstanding chemical and physical properties. $BaTiO_3$ is of major interest for applications as a ferroelectric material in capacitors and transducers.[11,12] Although $LiNbO_3$ does not crystallize in the perovskite structure, it is ferroelectric at room temperature, and its pronounced nonlinear optical properties make it promising for applications in optical communications and sensor systems.[13] $BaZrO_3$ has been investigated for special refractory applications.[14] The synthetic procedure is based on the dissolution of lithium or barium metal in benzyl alcohol and subsequent reaction with the corresponding metal alkoxide at temperatures between 200 and 220 °C. Benzyl alcohol has proved to be a versatile solvent and reactant for controlled crystallization and stabilization of oxidic nanoparticles.[15,16]

The powder X-ray diffraction (XRD) patterns of the as-synthesized materials are shown in Figure 1. All diffraction peaks in Figure 1a can be assigned to the $BaTiO_3$ phase without any indication of other crystalline by-products such as barium carbonate or titanium dioxide. The powder pattern in the $2\theta = 40$–$50°$ region is characteristic for the presence of either the cubic or tetragonal $BaTiO_3$ structure, and splitting of the 200 into tetragonal 200 and 002 reflections at about 45° is observed.[17] In this case, the reflections are too broad to discriminate between the two crystal modifications due to the small particle size. This was also confirmed by diffraction patterns calculated by the Debye equation of kinematic

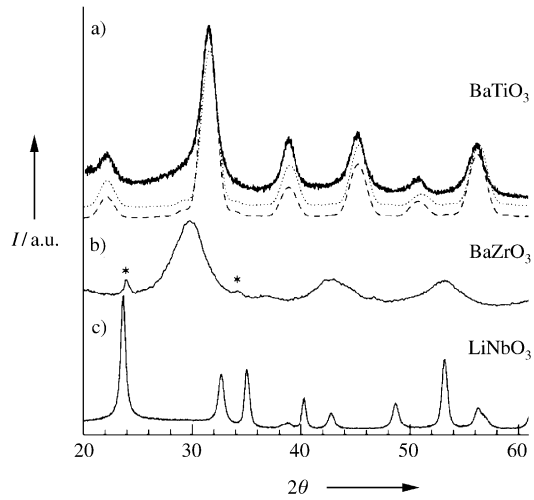

Figure 1. XRD patterns of a) $BaTiO_3$, b) $BaZrO_3$, and c) $LiNbO_3$ nanoparticles. Calculated diffraction patterns for spherical, monodisperse $BaTiO_3$ nanoparticles with diameters of 6 nm with the cubic (dotted line) and the tetragonal (dashed line) structure are shown in (a).

diffraction[18,19] for spherical, monodisperse particles with diameters of 6 nm. There are only minor differences between the cubic (Figure 1a, dotted line) and the tetragonal (Figure 1a, dashed line) powder patterns, and the calculated pattern of the tetragonal crystal modification does not display any splitting of reflections. The XRD pattern of $BaZrO_3$ is shown in Figure 1b. In addition to the perovskite phase, a small amount of $BaCO_3$ is also present (reflections marked with *). The broad peaks indicate small crystallite sizes on the nanometer scale. In contrast to the XRD diagrams of $BaTiO_3$ and $BaZrO_3$, $LiNbO_3$ gives rise to sharper reflections (Figure 1c). All peaks match with those of the pure $LiNbO_3$ phase.

Figure 2a shows an assembly of $BaTiO_3$ nanoparticles with an average particle size of 6 nm. This agrees well with the experimental and calculated XRD powder pattern. The lack of any surface-protecting layers results in some agglomeration of the particles. According to the randomly oriented lattice fringes, the particles have not coalesced. Figure 2b shows a selected-area electron diffraction (SAED) pattern. The lattice distances measured from the diffraction rings are in perfect agreement with the cubic and tetragonal modifications of the $BaTiO_3$ perovskite structure. Figure 2c and e show the HRTEM patterns of two isolated particles oriented along the [110] and [111] directions, respectively. The power spectrum (PS) of the particle in Figure 2c is shown in Figure 2d and provides evidence that the particles are well crystallized in the perovskite structure without the presence of defaults.

Figure 3a shows an overview TEM image of $BaZrO_3$ particles. In most cases, the primary particles are not isolated, but form wormlike agglomerates with diameters of 2–3 nm and lengths of up to 50 nm. Frequently, these worms assemble into larger, ball-like structures. The SAED pattern of such a spherical assembly (Figure 3b) shows broad rings that match with the $BaZrO_3$ structure. Furthermore, the HRTEM pattern (Figure 3c) shows that the lattice planes of the

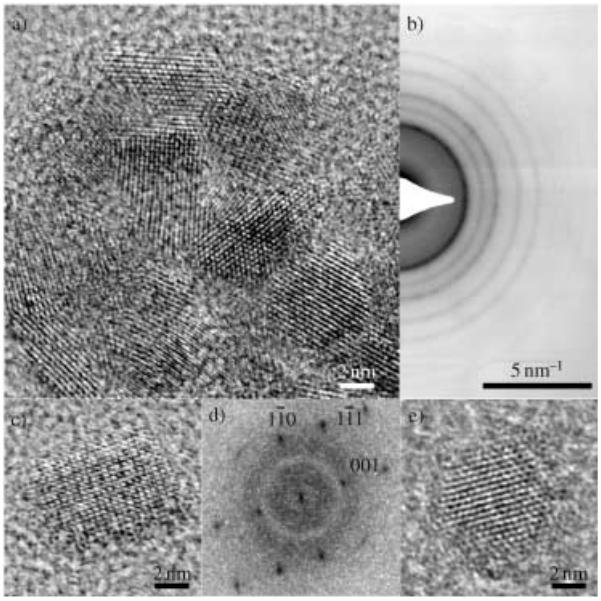

Figure 2. a) HRTEM image of an assembly of $BaTiO_3$ nanoparticles, b) SAED, c) and e) HRTEM of isolated particles, and d) PS of (c).

individual particles in the ball-like structure are randomly oriented with respect to each other. The HRTEM pattern of an isolated elongated particle proves the high degree of crystallinity (Figure 3d). This is further confirmed by the PS of this particle (Figure 3e), which is characteristic for the $BaZrO_3$ structure without structural defaults. The particle is aligned along the [111] direction. The selected HRTEM pattern of the large, spherical agglomerate and its PS (Figure 3f and g) show that the selected area represents the same structure and orientation as the isolated particle (Figure 3d), and thus provides evidence that the larger structures indeed consist of assembled $BaZrO_3$ nanoparticles.

Figure 4a shows an overview image of $LiNbO_3$ particles. They display a less uniform particle shape, and the sizes vary between 20 and 50 nm. The lattice distances measured from the SAED pattern (Figure 4b) coincide with those of the

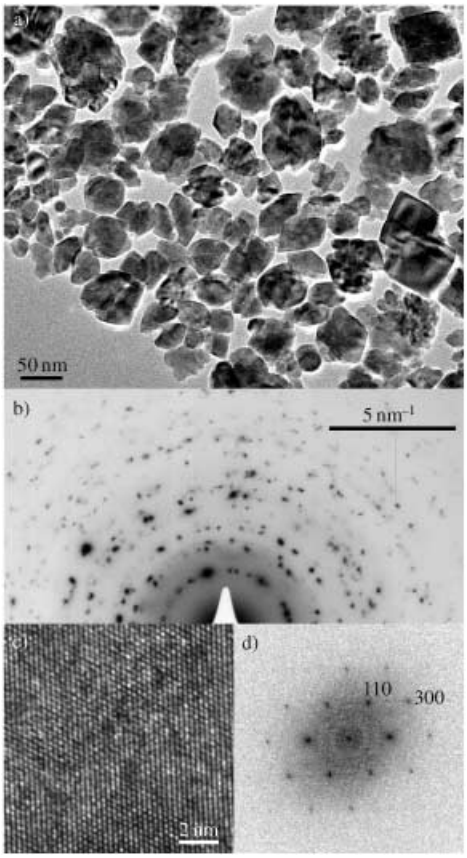

Figure 4. a) TEM image of $LiNbO_3$ nanoparticles, b) SAED, c) HRTEM of part of a particle, and d) corresponding PS.

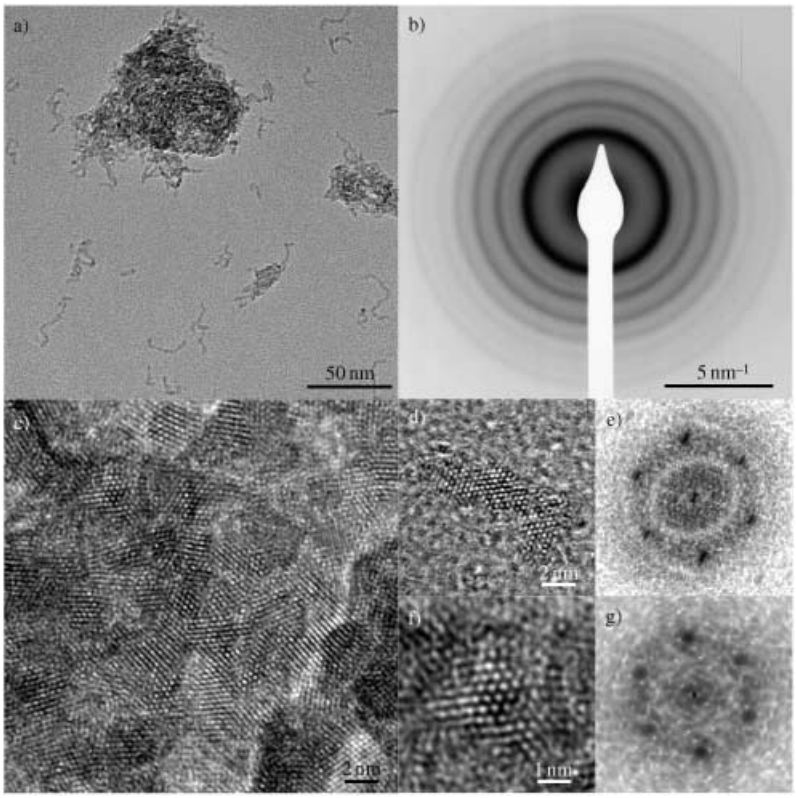

Figure 3. a) TEM image of $BaZrO_3$ nanoparticles, b) SAED, c) HRTEM of an assembly of particles, d) and f) HRTEM of isolated particles, and e) and g) corresponding PS.

$LiNbO_3$ structure. The HRTEM pattern of part of one particle shows several lattice planes with high crystallinity. The sharp reflections of its PS can be unambiguously attributed to the $LiNbO_3$ structure for a particle oriented along the [001] direction. In conclusion, structural studies performed on these materials prove that in all cases the particles are highly crystalline without any structural defaults, even for $BaZrO_3$ with a very small crystallite size.

At the moment, we can only speculate on the mechanism of formation of these nanomaterials. Since contact with water and air was carefully avoided by

performing the whole procedure in a glove box, we suggest that the reaction involves an aprotic condensation.[20] An oxo bridge could be formed by the reaction of two alkoxide groups bonded to two different metal centers by elimination of an organic ether. This ether-elimination route was postulated in the formation of a mixed-metal oxo alkoxide obtained from the reaction between titanium isopropoxide and lead isopropoxide,[21] but was never further developed. However, preliminary results show that other elimination reactions may also be involved in the formation of these compounds, and further investigations are under way.

We have presented a novel, generally applicable nonaqueous approach for the preparation of perovskite and $LiNbO_3$ nanoparticles in gram quantities. The synthetic protocol is based on the dissolution of alkali or alkaline earth metals in benzyl alcohol and subsequent reaction with transition metal alkoxides at relatively low temperatures of 200–220 °C. All the as-synthesized particles are highly crystalline, and the particles are among the smallest reported so far for these compounds. Since electroceramic materials are following a similar trend to miniaturization as conventional semiconductors, the synthesis of nanosized oxidic building blocks is moving into the focus of scientific and technological interest. Ferroelectrics are a particularly promising class of materials for the fabrication of electronic devices, as they are already an integral part of modern nanotechnological operations.

Experimental Section

Materials: Titanium(IV) isopropoxide (Aldrich, 99.999 %), zirconium(IV) isopropoxide isopropanol complex (Aldrich, 99.9 %), niobium(V) ethoxide (Strem, 99.9 + %), barium metal (Aldrich, 99.99 %), lithium metal (Aldrich, 99.9 + %), and anhydrous benzyl alcohol (Aldrich, 99.8 %) were used without further purification. For the solvothermal treatment Parr acid-digestion bombs with 45 mL Teflon cups were used.

Synthesis: All procedures were carried out in a glove box (O_2 and $H_2O < 0.1$ ppm). In a typical synthesis of $BaTiO_3$ or $BaZrO_3$, 3.6 mmol of Ba was stirred in a vial with 25 mL of benzyl alcohol at slightly elevated temperature (ca. 50 °C) until completely dissolved. One molar equivalent of $Ti(OiPr)_4$ or $Zr(OiPr)_4{\cdot}HOiPr$ was added to the solution. The reaction mixture was stirred for another few minutes and then transferred into the autoclave. The autoclave was taken out of the glove box and heated in a furnace ($BaTiO_3$: 200 °C for ca. 48 h; $BaZrO_3$: 200 °C for 3 d and another 3 d at 220 °C). In the case of $LiNbO_3$, 2.16 mmol of Li was dissolved in 25 mL of benzyl alcohol and subsequently mixed with one molar equivalent of $Nb(OEt)_5$. The solution was heated in an autoclave at 220 °C for 4 d. The resulting milky suspensions were centrifuged, and the precipitates thoroughly washed with ethanol and diethyl ether and subsequently dried in air at 60 °C overnight.

Characterization: The XRD diagrams of all samples were measured in reflection mode ($Cu_{K\alpha}$ radiation) on a Bruker D8 diffractometer equipped with a scintillation counter. TEM images were recorded on a Philips CM200 FEG microscope operated at 200 kV.

Received: November 11, 2003 [Z53300]

Keywords: nanostructures · perovskite phases · scanning probe microscopy · solvothermal synthesis

[1] M. E. Lines, A. M. Glass, *Principles and Applications of Ferroelectrics and Related Materials*, Oxford University Press, Oxford, **2001**.
[2] C. D. Chandler, C. Roger, M. J. Hampden-Smith, *Chem. Rev.* **1993**, *93*, 1205.
[3] M. Veith, S. Mathur, N. Lecerf, V. Huch, T. Decker, H. P. Beck, W. Eiser, R. Haberkorn, *J. Sol-Gel Sci. Technol.* **2000**, *17*, 145.
[4] I. J. Clark, T. Takeuchi, N. Ohtori, D. C. Sinclair, *J. Mater. Chem.* **1999**, *9*, 83.
[5] E. Ciftci, M. N. Rahaman, M. Shumsky, *J. Mater. Sci.* **2001**, *36*, 4875.
[6] R. I. Walton, F. Millange, R. I. Smith, T. C. Hansen, D. O'Hare, *J. Am. Chem. Soc.* **2001**, *123*, 12547.
[7] H. J. Chen, Y. W. Chen, *Ind. Eng. Chem. Res.* **2003**, *42*, 473.
[8] S. O'Brien, L. Brus, C. B. Murray, *J. Am. Chem. Soc.* **2001**, *123*, 12085.
[9] M. J. Pooley, A. V. Chadwick, *Radiat. Eff. Defects Solids* **2003**, *158*, 197.
[10] F. Boschini, B. Robertz, A. Rulmont, R. Cloots, *J. Eur. Ceram. Soc.* **2003**, *23*, 3035.
[11] T. M. Shaw, S. Trolier-McKinstry, P. C. McIntyre, *Annu. Rev. Mater. Sci.* **2000**, *30*, 263.
[12] A. S. Bhalla, R. Guo, R. Roy, *Mater. Res. Innovations* **2000**, *4*, 3.
[13] M. Lawrence, *Rep. Prog. Phys.* **1993**, 363.
[14] B. Robertz, F. Boschini, R. Cloots, A. Rulmont, *Int. J. Inorg. Mater.* **2001**, *3*, 1185.
[15] M. Niederberger, M. H. Bartl, G. D. Stucky, *Chem. Mater.* **2002**, *14*, 4364.
[16] M. Niederberger, M. H. Bartl, G. D. Stucky, *J. Am. Chem. Soc.* **2002**, *124*, 13642.
[17] M. H. Frey, D. A. Payne, *Phys. Rev. B* **1996**, *54*, 3158.
[18] W. Vogel, *Cryst. Res. Technol.* **1998**, *33*, 1141.
[19] N. Pinna, U. Wild, J. Urban, R. Schlögl, *Adv. Mater.* **2003**, *15*, 329.
[20] A. Vioux, *Chem. Mater.* **1997**, *9*, 2292.
[21] S. Daniele, R. Papiernik, L. G. Hubert-Pfalzgraf, S. Jagner, M. Hakansson, *Inorg. Chem.* **1995**, *34*, 628.

